Drag forces and unsteady wakes behind a poro-elastic membrane disk

Alexander Gehrke, Zoe King, and Kenneth S. Breuer*
Center for Fluid Mechanics, Brown University, Providence, USA[1]
*Correspondence: *kbreuer@brown.edu*

In nature, most passive and active structures are flexible. Plant leafs and seeds deform with the wind to reduce structural loads or increase their dispersion range [1]. Insects, birds, and bats have passively and actively compliant wings that help them to generate thrust and manoeuvre. In addition some bird feathers are porous which has been shown to reduce noise emissions due to the suppression of coherent vortex shedding [3]. Despite all the benefits in the natural examples elastic, and especially poro-elastic, structures are rarely employed in human engineered devices. Complex fluid-structure interactions especially at varying flow conditions give rise to a large number of parameters making the scaling and design difficult. Recently, Mathai et al. [2] investigated the kinematics and dynamics of highly compliant membrane disks in wind tunnel experiments and found that the membrane's oscillations increase the turbulent kinetic energy in the wake which leads to increased steady and unsteady drag production. In contrast, at a much lower Reynolds number, Cummins et al. [1] found that porous dandelion seeds, consisting of a bundle of drag-enhancing bristles, stabilized a coherent vortex in the wake which maximizes the aerodynamic loading while minimizing material requirements.

While there are several theoretical studies predicting aerodynamic and aeroacoustic benefits of poro-elasticity materials, systematic experimental investigations and scaling of the poro-elastic phenomenon are still missing. In this study, we report on the effects of poro-elasticity on thin, circular membrane disks, and measure the deformation and drag force acting on the membrane for varying levels of porosity. The membranes are made from a hyper-elastic elastomer (*Dragon Skin FX Pro-Shore Hardness 2A, Smooth-On Inc., Macungie, PA*) and have a thickness of $h = 0.6$ mm. A laser cutter is used to fabricate the different porosity patterns (shown in fig. 1(h)) with a pore diameter of $d = 2$ mm. For the wind tunnel experiments, the membranes are mounted on a "claw" that positions the membranes head-on to a free stream flow (fig. 1(c)). The aerodynamic forces are measured using a six-axis force-torque transducer (*Nano17, ATI Industrial Automation, USA*) mounted at the base of the claw for all 5 porosity patterns at different flow velocities ($U_\infty = 9 - 38$ m/s). The shape of the membrane is reconstructed from high-speed, multiple-camera measurements of a set of markers distributed on the membrane.

[1]This work was supported by NSF under grant number GR5260547

Results

When the compliant membranes are subject to a pressure loading they deform to a spherical cap shape with a maximum deflection w_0 at the center [fig. 1(a,c)]. All tested porosity patterns lead to the same deformation w_0 as function of the dynamic pressure ($0.5\rho U_\infty^2$) despite greatly varying levels of porosity [fig. 1(d)]. The deformation thus is mainly affected by the material properties, the shear modulus G_m and the thickness, h, of the membrane, and the pressure difference ($\Delta p = p_e - p_i$). Neglecting the porosity allows us to express the balance between tension in the membrane, T, and the dynamic pressure with the aeroelastic number [fig. 1(b)] in the following way:

$$Ae = \frac{\text{Tension}}{\text{Pressure}} = \frac{T}{p_e - p_i} = \frac{T}{0.5\rho U_\infty^2 D} \,. \tag{1}$$

The tension for any section of the membrane is derived from the first Piola-Kirchhoff stress under bi-axial loading:

$$T = G_m h \left(1 - \frac{1}{\lambda^6}\right) \tag{2}$$

where λ is the membrane stretch. We use a two-parameter Gent model that accounts for the strain-stiffening and strain-softening behavior of the elastomer seen for the hyper-elastic material used in this study [fig. 1(d)] [4]. The membrane deformation, w_0, follows a power law as a function of the aeroelastic number, Ae, and captures the strain-softening of the hyper-elastic material [fig. 1(e)]. Further details about the aeroelastic scaling and its derivation are outlined in [2,4].

The average drag coefficient acting on the membrane:

$$C_d = \frac{F_d}{\frac{1}{8}\pi\rho U_\infty^2 D^2}, \tag{3}$$

is presented in fig. 1(f) as a function of the deformation w_0/D for the varying levels of porosity. The drag coefficient increases monotonically with deformation for the non-porous disk in agreement with previous experiments [2]. However, porosity decreases the drag coefficient, which exhibits a negative slope with increasing deformation for initial porosities $\phi > 0.9\%$. A drag reduction of up to 20% relative to the non-porous disk is achieved for the highest initial porosity $\phi = 6.6\%$.

We find similar trends for drag fluctuations expressed as the

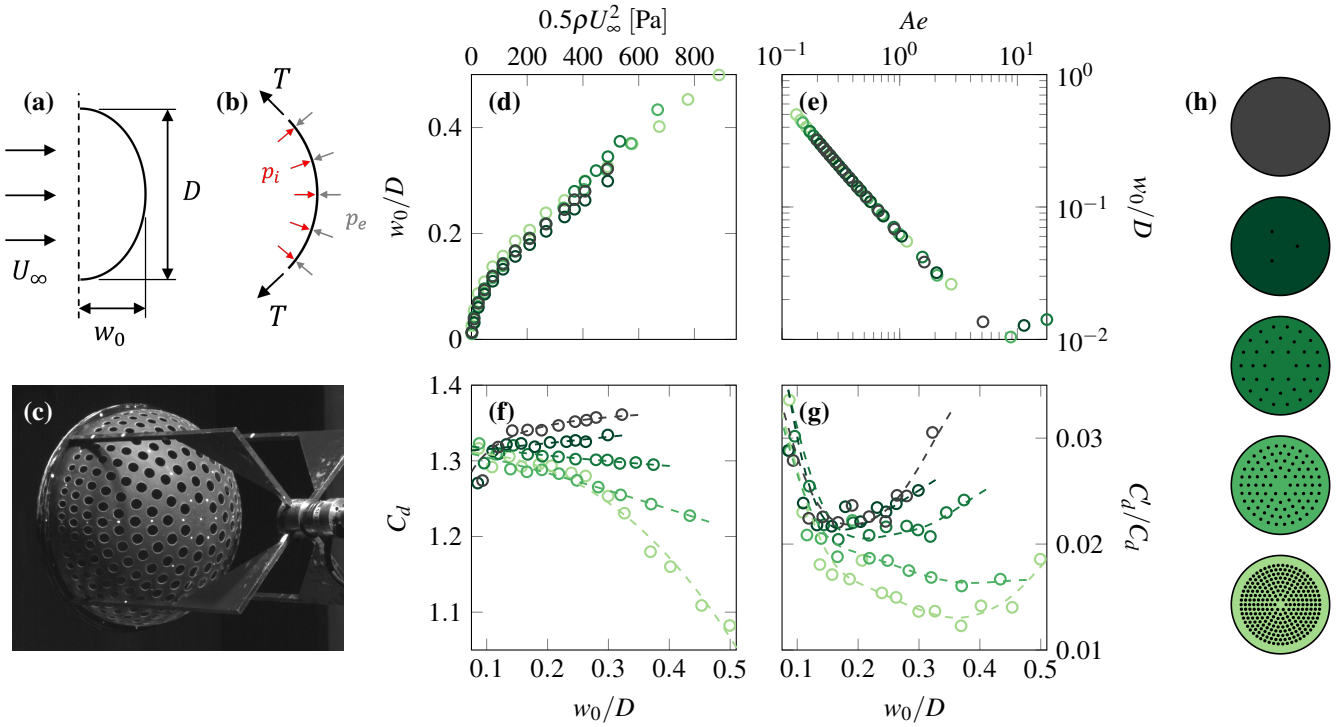

Figure 1: (a) Sketch of the compliant membrane dimensions, and (b) of the relationship between pressure and tension. (c) Example of the poro-elastic membrane deformation in the wind tunnel. (d) Membrane deformation as a function of the dynamic pressure, and (e) membrane deformation as a function of the Aeroelastic number. (f) Average drag coefficient, and (g) drag coefficient fluctuation plotted over the membrane deformation. (h) Overview of the different porosity patterns tested in this study. The colors in d-f correspond to the different fractions of porosity of the undeformed membranes: $\phi = 0, 0.2, 0.9, 2.2, 6.6\%$.

normalized standard deviation of the drag coefficient C_d'/C_d, [fig. 1(g)]. At low deformations the drag fluctuations, C_d', are similar for all compliant membranes. However, the non-porous disks experience significantly higher fluctuations at large deformations w_0/D, and the fluctuations are reduced as the porosity increases. A reduction of more than 50% is observed for most porous disks for the same membrane shape of $w_0/D = 0.32$.

Discussion

In this study, we investigated the effects of poro-elasticity on the unsteady deformation and drag forces on circular disks in wind tunnel experiments. The shape and drag production was measured for varying levels of porosity and non-porous elastic disks for reference. The average shape of the deformed membranes is a spherical cap and depends mainly on the material properties and the applied pressure, but not the porosity (at least for the relatively low porosities considered here). We scale the equilibrium between the tension and the pressure on the membrane assuming bi-axial loading and a two parameter Gent model to describe the hyper-elastic material behavior. The model captures the relationship between membrane shape and dynamic pressure well, and reveals a power law between the deformation and the aeroelastic number Ae. The drag force coefficient increases at larger membrane deformations both in terms of the average force C_d and the force fluctuations C_d' for the non-porous membranes. An overall reduction of the averaged and time-varying drag forces is observed with increasing levels of porosity. In similar experiments, strong membrane vibrations were identified as a key mechanism responsible for increased turbulent kinetic energy production and drag force fluctuations on non-porous membranes [2]. Our results suggest that poro-elasticity stabilizes the turbulent wake over the membrane which reduces the membrane vibrations and the unsteady drag production on the deformed disks, similar to the effects of dandelion seeds or bird feathers observed in nature [1, 3]. Our findings can shed further insights into the fluid-structure interaction of poro-elastic structures in nature and pave the way for novel engineering designs for example in parachutes or micro air vehicles.

References

[1] Cummins, Cathal, Madeleine Seale, Alice Macente, Daniele Certini, Enrico Mastropaolo, Ignazio Maria Viola, and Naomi Nakayama. A Separated Vortex Ring Underlies the Flight of the Dandelion. *Nature*, 562, no. 7727: 414–18, 2018.

[2] Mathai, Varghese, Asimanshu Das, Dante L. Naylor, and Kenneth S. Breuer. Shape-Morphing Dynamics of Soft Compliant Membranes for Drag and Turbulence Modulation. *Physical Review Letters*, 131, no. 11: 114003, 2023.

[3] Jaworski, Justin W., and Nigel Peake. Aeroacoustics of Silent Owl Flight. *Annual Review of Fluid Mechanics*, 52, no. 1: 395–420, 2020.

[4] Das, Asimanshu, Kenneth S. Breuer, and Varghese Mathai. Nonlinear Modeling and Characterization of Ultrasoft Silicone Elastomers. *Applied Physics Letters*, 116, no. 20: 203702, 2020.